

# A “Self-checking” Algorithm for Accurate Detection of High-density and Fast-moving Vesicles in Time-series Fluorescence Images\*

ZHANG Xiang<sup>1,2)\*\*</sup>, LIU Xin-Yi<sup>2)</sup>, LÜ Ping-Ping<sup>2)</sup>, JIA Ce<sup>2)</sup>

<sup>1)</sup> College of Life Science and Technology, Huazhong University of Science and Technology, Wuhan 430074, China;

<sup>2)</sup> Institute of Biophysics, Chinese Academy of Sciences, Beijing 100101, China)

**Abstract** This paper proposed the “self-checking” algorithm to improve the detection accuracy of multiple moving targets in time-series fluorescence images, such as vesicles. The main idea of this algorithm is to construct a multi-kernel function superposition model and use the model to fit the data at the indistinguishable moment; the number of vesicles and the central positions of vesicles are determined from the set based on  $\chi^2$ -statistics of the residuals in least-square fits of the models to the image data. By comparing the detection accuracy with or without the “self-checking” algorithm in simulated images, we found that the detection accuracy with the “self-checking” algorithm was improved significantly. Meanwhile, we proposed an optimized flow chart of vesicle tracking which was applied to analyze the vesicles in mice  $\beta$  cells. We found that the number of vesicle traces will increase and the average docking time of vesicles will decrease after glucose stimulation based on our tracking analysis. This is because  $\beta$  cells will release insulin to regulate glucose balance with the help of vesicle translocation and secretion after glucose stimulation. In a word, we quantified the vesicles activity in mice  $\beta$  cell by tracking analysis on subcellular level.

**Key words** self-checking algorithm, vesicle tracking, vesicle detection, time-series images

**DOI:** 10.16476/j.pibb.2017.0046

In a biological study, it is often necessary to observe the dynamic movement of vesicles in cells; when we mark vesicles with fluorescent protein, the dynamic movement of vesicles can be recorded by a total internal reflection fluorescence microscope. Then, we can obtain much valuable information through the analysis of the dynamic movement of vesicles<sup>[1-3]</sup>. Because manually analyzing a large number of vesicles is time-consuming and exhausting, automatic algorithms are necessary to speed up the process<sup>[4-5]</sup>. Many methods are used to detect the spot signal<sup>[6]</sup>, such as the adaptive threshold algorithm, which divides a gray level image into the background and target according to the maximum between-cluster variance<sup>[7]</sup>. The larger the between-cluster variance between the background and target, the more different the two parts of the image will be; if some targets are wrongly classified as the background or some backgrounds are wrongly classified as the target, the

difference between the two parts will be smaller. Therefore, the segmentation for maximum between-cluster variance indicates the minimum probability of misclassification. However, this global threshold method cannot obtain truly satisfactory results for biological fluorescence images because the signal and background in biological fluorescence images are inhomogeneous<sup>[8]</sup>. This means that the signal in one part of the image can be brighter or darker than the background in another part. To overcome this problem, the top hat algorithm based on morphology was proposed<sup>[9]</sup>. This algorithm first carries out the erosion operation for an image to filter

\*This work was supported by a grant from The National Natural Science Foundation of China (31300701).

\*\*Corresponding author.

Tel: 86-10-64888523, E-mail: zhangxiang@ibp.ac.cn

Received: February 13, 2017 Accepted: March 30, 2017

out the spots in images and lower the overall brightness of the image and then carries out the dilation operation to restore the area and brightness of the light background; finally, it subtracts the processed image from the original image to obtain the filtered image. A more robust algorithm was proposed that is based on multi-resolution analysis<sup>[8]</sup>. This algorithm first applies the  $\acute{a}$  trous wavelet transform to the image and then calculates the median absolute deviation  $\sigma$  of each coefficient<sup>[10]</sup>, with  $t=k\sigma/0.67$  as the threshold value for each coefficient filtering<sup>[11]</sup>, and finally reconstructs the image by using the product of each coefficient. Many paper showed that the algorithm was robust in detecting spots in biological fluorescence images<sup>[12-14]</sup>. This algorithm was used to track small particles in fluorescence images<sup>[15-16]</sup>. However, if two spots are too close, the algorithm will be unable to distinguish them. This is an inevitable problem for threshold segmentation algorithms.

The local maximum algorithm was put forward to detect spots with small distances<sup>[17]</sup>. This algorithm is defined as follows: if a pixel is brighter than the other pixels around it within the distance range  $w$ , then this pixel will be regarded as the local maximum value. This algorithm was used to track spots in fluorescence images<sup>[18-19]</sup>. The watershed algorithm was put forward to detect spots with small distances<sup>[20]</sup>. The watershed algorithm regards the image as a “topographic map”, among which the areas with strong brightness have higher pixel values, and the areas with weak brightness have lower pixel values. It carries out the image segmentation by finding the “catchment basin” and “watershed boundary”. Although these two algorithms are able to detect spots within small distances of each other, we found that the detection accuracy dramatically decreases as the distance gets smaller. The above situation will occur frequently in fluorescence images during the motion of vesicles, and if detection is wrong, an error result will be obtained after automatic analysis of the vesicles’ dynamic movements. Therefore, we proposed the “self-checking” algorithm to improve the detection accuracy of multiple moving targets in time-series images, such as vesicles. The idea of the algorithm is that two vesicles which are close together at some time are difficult to distinguish, but these vesicles are in a state of motion, and the distance between them will be large enough to help us distinguish them at some other time. This algorithm first constructs a multi-kernel

function superposition model and then uses the model to fit the data at the indistinguishable moment before finally determining the number of vesicles and the central positions of vesicles from the set based on the  $\chi^2$ -statistics of the residuals in least-square fits of the models to the image data.

## 1 Methods

### 1.1 Algorithm

When analyzing the vesicle dynamic movement in fluorescence images, we find that vesicle movement can be roughly divided into three types of motion states<sup>[1, 21-22]</sup>: single direction motion state, random motion state and “Cage” motion state. The “Cage” motion state refers to when the vesicle is limited to some location or has tiny swing at some location. It shall correctly detect the entire path of the vesicle to analyze the vesicle’s dynamic movement. However, at the cell surface, a large number of vesicles in motion will inevitably be close to one another or overlap. In this case, the application of the traditional adaptive threshold algorithm and top hat algorithm to an image is unable to solve the above problem, even when using the wavelet transform algorithm. Using the local maximum algorithm and watershed algorithm can separate a portion of the vesicles, but the detection accuracy is low. To improve the detection accuracy, we find solutions from image sequences. Two vesicles that are close together at some time are difficult to distinguish, but these vesicles are in a state of motion, and the distance between them will be large enough to help us distinguish them at some other time. Therefore, we constructed a multi-kernel function superposition model and then used this model to fit the data at the indistinguishable moment; finally, the number of vesicles and the central position of vesicles were determined from the set based on the  $\chi^2$ -statistics of the residuals in least-square fits of the models to the image data.

First, we construct a multi-kernel function superposition model

$$f(x, y, n) = \sum_{i=1}^n g(x, y) \quad (1)$$

where  $g(x, y)$  is the kernel function. Because the vesicles in fluorescence images are indicated by the superimposed point spread function (PSF) of the microscope imaging system, the kernel function can be approximated by using a Gaussian distribution for the 2D case.

$$g(x, y) = a \exp\left(-\frac{(x-c)^2 + (y-d)^2}{2\sigma^2}\right) \quad (2)$$

Putting equation (2) into equation (1), we can obtain  $f(x, y, n)$  as follows

$$f(x, y, n) = \sum_{i=1}^n a_i \exp\left(-\frac{(x-c_i)^2 + (y-d_i)^2}{2\sigma_i^2}\right) + b \quad (3)$$

In this model, where  $n$  is the number of Gaussians,  $c_i$  is the center position of each Gaussian in the  $x$ -axis direction,  $d_i$  is the center position of each Gaussian in the  $y$ -axis direction,  $a_i$  is the amplitude of each Gaussian,  $b$  is the background value, and  $\sigma_i$  is the standard deviation of each Gaussian. In practice, when calculating a discrete approximation of a Gaussian, approximately  $3\sigma_i$  outside the range can be ignored.

We set the width of slide window  $L=2$ , and images of the entire time series can be divided into collection  $\{I_k, I_{k+1}\}_{k=1}^{N-1}$ , where  $I_k$  is the image data in frame  $k$ , and  $N$  is the total number of frames. There is  $D_{k,j}$  ( $j = 1, 2 \dots M$ ) for each  $I_k$ , where  $D_{k,j}$  represents detected particles in frame  $k$ , and  $M$  is the number of detected particles in frame  $k$ . For each  $D_{k,j}$ , the center coordinate is  $(x_{k,j}, y_{k,j})$ . We can cut out the sub image  $B_{k,j}$  from  $I_k$  with  $(x_{k,j}, y_{k,j})$  as the center and  $R$  as the radius. In our experiment we set  $R=5$  which is big enough to contain the particles. The number of detected particles in  $B_{k,j}$  and  $B_{k+1,j}$  are  $n_k$  and  $n_{k+1}$ , respectively. Next, we compare  $n_k$  and  $n_{k+1}$ . If  $n_k$  is equal to  $n_{k+1}$ , then the same number of particles are found in two adjacent images, and no process is needed. If  $n_k$  is greater than  $n_{k+1}$ , then we need to determine whether it is really one point less or whether the two points are too close to be identify correctly. Thus, we fit  $B_{k+1,j}$  with  $f(x, y, n_k)$  and  $f(x, y, n_{k+1})$  to obtain the residues  $R_{k+1,j}^{n_k}$  and  $R_{k+1,j}^{n_{k+1}}$ . If  $R_{k+1,j}^{n_k}$  is less than  $R_{k+1,j}^{n_{k+1}}$ , it indicates that there are more  $n_k$  than  $n_{k+1}$  points in  $B_{k+1,j}$ . Fitting parameters  $a_i, b, c_i, d_i$ , and  $\sigma_i$  need to be limited to a reasonable range to further confirm this judgment. Finally, we use fitting center points  $(c_i, d_i)$  to replace the original center points in  $B_{k+1,j}$ . Conversely, if  $n_k$  is less than  $n_{k+1}$ , we can perform a similar process to replace the original center points in  $B_{k,j}$  with fitting center points  $(c_i, d_i)$ .

### 1.2 Simulated images construction

First, we test the effectiveness of the algorithm through a series of standard simulated images. Then, we generate a series of 100 frames time sequence images with a size of  $256 \times 256$  and place each vesicle's

generation into the time series image one by one; the number and maximum movement speed of vesicles will also serve as parameter settings. We use a 2D Gaussian to simulate the vesicles' distribution of fluorescence intensity; the radius of each vesicle is a fixed pixel value, and the vesicles' initial positions and the lengths of their motion trajectories will be generated at random. Moreover, the direction and speed of vesicles' motion trajectories are generated randomly for each frame. We generate vesicles with three types of motion states and generate them in the images with a certain proportion: one third single direction motion, one third random motion and one third "Cage" motion.

### 1.3 Islet $\beta$ cell isolation and labeling

Islet  $\beta$  cells were isolated from C57/6J mice (Nanjing Model Animal Experiment Center). First, the pancreas was separated and digested in collagenase (Sigma, America, 0.5 g/L in Hank's) for 20 min. Then, islets that appeared to be globular or rod-like under a stereoscope were sorted and cultivated in a  $\beta$  cell culture medium overnight at  $37^\circ\text{C}$ . The  $\beta$  cell culture medium was made using RPMI 1640 with L-glutamine containing 10% heat-inactivated fetal bovine serum (FBS; from Wisent, Canada), 11.2 mmol/L glucose, 1% ( $v/v$ ) 100 U/ml penicillin and 100 g/L streptomycin. The islets were washed with Hank's and digested with pancreatin for 3 min. Then, the  $\beta$  cells were re-suspended in the  $\beta$  cell culture medium and then seeded onto 18-mm glass coverslips (Fisher Scientific, America) at 30 islets/coverslip. Adenovirus, which carries the NPY-EGFP (NPY is a neuropeptide which is composed of 36 amino acids; NPY can be wrapped in the form of cargo in the insulin vesicles, so it is often used to mark the insulin vesicles<sup>[23]</sup>) DNA sequence (SinoGenoMax, China), was added into the culture medium at a concentration of  $1 \mu\text{l}/10 \text{ ml}$  for labeling. After 6 h of incubation, the culture medium was replaced with a fresh medium.

### 1.4 TIRM imaging

After 12–24 h of infection, the  $\beta$  cells were transferred to a chamber filled with Krebs-Ringer HEPES buffer (KRBB) for imaging. The experiments were performed at  $30^\circ\text{C}$ . Time-series images were acquired by the total internal reflection fluorescence microscopy (TIRFM) imaging system, which was constructed based on the prismless and through-the-lens configuration, as previously described<sup>[5]</sup>. The TIRFM imaging system was equipped with a  $150 \times$ ,

1.45 NA oil-immersion objective (Olympus, Japan), EMCCD camera (Andor iXon 897, England), and lasers (Coherent, America). The EMCCD camera was driven by Andor Solis (Andor, England). A 488-nm laser was used to excite fluorescence during the experiment.

## 2 Results

We choose the wavelet transform algorithm, local maximum algorithm and watershed algorithm to compare and verify the effectiveness of the algorithm through analyzing the correct detection of vesicle proportion before and after the self-check algorithm process. The accuracy  $P$  is calculated as follows.

$$P = \left( 1 - \frac{FP(n) + FN(n)}{N_{\text{Total}}} \right) \times 100\% \quad (4)$$

where  $N_{\text{Total}}$  is the total number of test vesicles.  $FP(n)$  is the number of false positives, which means that the number of detected spots is more than the number of ground truths.  $FN(n)$  is the number of false negatives, which means that the number of detected spots is less than the number of ground truths. False positives and false negatives are identified manually.

We adopt EMCCDD (iXon 897, Andor, England) with a pixel size of 16  $\mu\text{m}$  and an objective lens with a

magnification of 150 $\times$ ; therefore, the pixel size in the image is approximately 107 nm. The radius of the simulated vesicle is 3 pixels, and the accuracy of the three algorithms reaches up to 100% for vesicles with a distance above 6 pixels. That is, if the distance between two vesicles is large enough, they can be detected correctly. Therefore, the accuracy of these algorithms for distances below 6 pixels must be determined. The simulated vesicle images with different distances is shown in Figure 1(a)–(f) show the two-dimensional simulated vesicle images, with a central distance ranging from 1 pixel to 6 pixels. (g)–(l) corresponds to the intensity distribution graph of (a)–(f). From Figure 1, we can see that two vesicles can be detected correctly through setting the proper threshold when the distance is 4 pixels and 5 pixels. If the distance between two vesicles is within 3 pixels, the vesicles cannot be detected correctly through simply setting a threshold. Therefore, we take the information of the time series image into consideration to recognize the vesicles, which is the purpose of our algorithm. Because the algorithm is a verification process based on the recognition completion of other algorithms, we call this algorithm the self-checking (SC) algorithm.

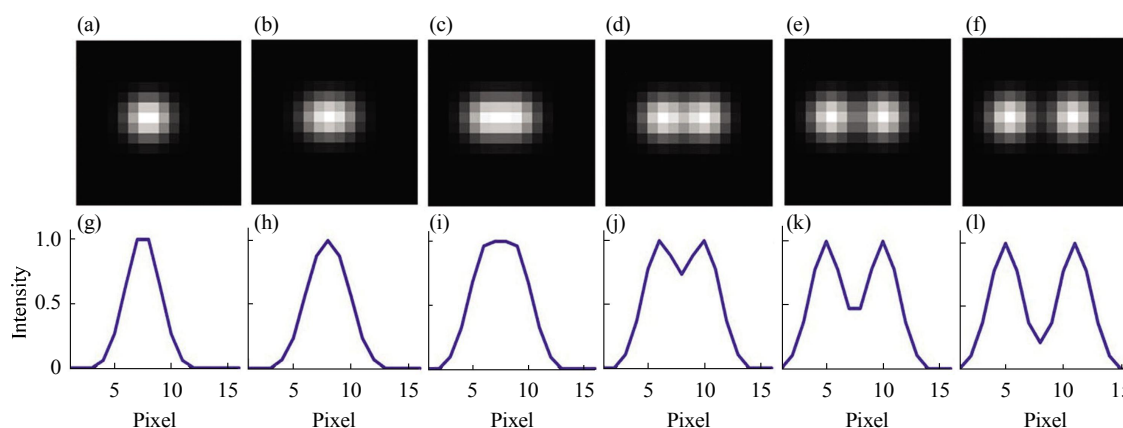


**Fig. 1 Simulated vesicle images with different distances**

(a)–(f) The two-dimensional simulated vesicle images, with a central distance ranging from 1 pixel to 6 pixels. (g)–(l) corresponds to the intensity distribution graph of (a)–(f).

We can see from Figure 2 that the traditional threshold segmentation algorithm, taking the wavelet transform algorithm as the example in the paper, has a recognition accuracy close to 0% for vesicles with distances within a pixel interval of [1, 6), whereas the detection accuracy is 100% for pixel intervals of

[6,  $+\infty$ ). However, the local maximum algorithm and watershed algorithm have a detection accuracy of 100% within a pixel interval of [5,  $+\infty$ ); the detection accuracy is gradually reduced for less than 5 pixels. The local maximum algorithm has a detection accuracy of 70.8% within a pixel interval of [4, 5),

7.7% within a pixel interval of [3,4), 6.1% within a pixel interval of [2,3), and 1.2% within a pixel interval of [1,2). For the watershed algorithm, the detection accuracy is 86.2% within a pixel interval of [4,5), 47.6% within a pixel interval of [3,4), 0.5% within a pixel interval of [2,3), and 0% within a pixel interval of [1,2). Thus, it can be seen that the recognition accuracy of the watershed algorithm is better than that of the local maximum algorithm within the pixel interval of [3,5), whereas the watershed algorithm is worse than the local maximum algorithm within the pixel interval of [1,3). When adding the self-checking algorithm, the accuracy of each algorithm improves greatly. The wavelet transform algorithm plus the self-checking algorithm has an accuracy of 79.7% within the pixel interval of [5,6), 63% within the pixel interval of [4,5), 52% within the pixel interval of [3,4), 48.6% within the pixel interval of [2,3), and 19.5% within the pixel interval of [1,2). The local maximum algorithm plus the self-checking algorithm has an accuracy of 97.8% within the pixel interval of [4,5), 93.9% within the pixel interval of [3,4), 82.1% within the pixel interval of [2,3), and 42.8% within the pixel interval of [1,2). The watershed algorithm plus the self-checking algorithm has an accuracy of 99.5% within the pixel interval of [4,5), 96.7% within the pixel interval of [3, 4), 84.3% within the pixel interval of [2,3), and 45.1% within the pixel interval of [1,2). Therefore, the detection accuracy obtained by the watershed algorithm plus the self-checking algorithm is the best overall.

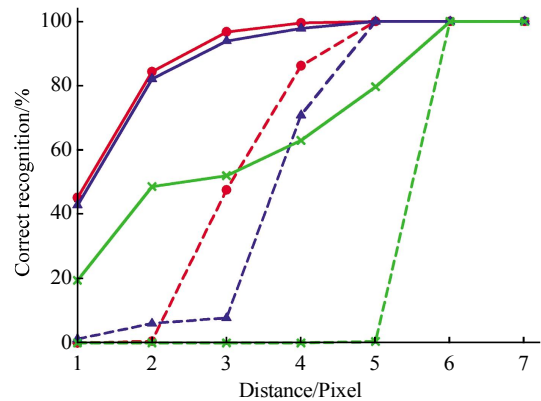


**Fig. 2 Comparison of different algorithms on detection accuracy at different distances**

Comparison of the detection accuracy of the wavelet transform algorithm, local maximum algorithm and watershed algorithm, as well as these algorithms plus the self-checking algorithm. The abscissa 1 represents the pixel interval of [1,2), and 2 represents the pixel interval of [2,3), and so on. Testing data is 20 groups of 100 frames time sequence images with a size of 256×256. The number of vesicles is 40 and the maximum movement speed is 3 pixels per frame in each group. ●---●: Watershed; ●---●: Watershed+SC; ▲---▲: Local maximum; ▲---▲: Local maximum+SC; ×---×: Wavelet; ×---×: Wavelet+SC.

As shown in Figure 3, we also test the detection accuracy of the watershed algorithm and watershed algorithm plus the self-checking algorithm under different parameters. Figure 3a uses the testing data to randomly generate three groups of time series images with different vesicle quantities; the vesicle quantities for each group of data are 30, 40, 50 in order, and the maximum movement speed is 3 pixels for each frame.

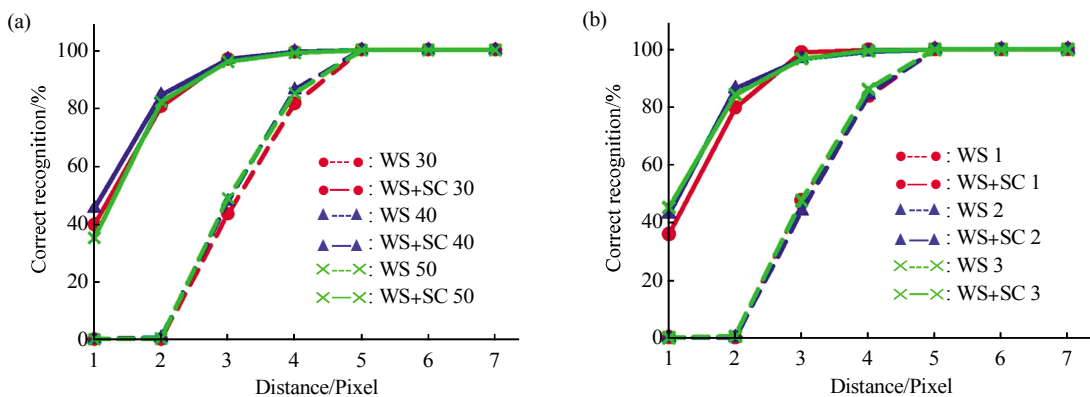


**Fig. 3 The detection accuracy of the watershed algorithm and watershed algorithm plus the self-checking algorithm under different parameters**

Testing data are used in (a) to randomly generate three groups of time series images with different vesicle quantities; the vesicle quantities for each group of data are 30, 40, 50 in order, and the maximum movement speed is 3 pixels for each frame. Testing data are used in (b) to randomly generate three groups of time series images with different maximum movement speeds; the vesicle quantity in each group of data is 40, with the maximum movement speed being 1, 2 and 3 pixels per frame, respectively.

Testing data are used in Figure 3b to randomly generate three groups of time series images with different maximum movement speeds; the vesicle quantity in each group of data is 40, with the maximum movement speed being 1, 2, and 3 pixels per frame, respectively. From Figure 3, it can be seen that different vesicle quantities and maximum speeds have no effect on the algorithm's detection accuracy and that the watershed algorithm plus the self-checking algorithm can obtain a high detection accuracy under different parameters.

We also add different levels of Gaussian noise to the time series images to test the detection precision of

the self-checking algorithm. First, we use the wavelet transform algorithm to remove noise and then carry out the detection using the watershed algorithm plus the self-checking algorithm. We determined the bias of only the self-checking algorithm. Bias is determined by the difference between the detected center and the real center. As shown in Figure 4, when the signal-to-noise ratio (SNR) is 1, the average bias is 0.0423 pixels. Increasing the signal-to-noise ratio will make the bias smaller ( $SNR = I_s / \sigma_N$ , where  $I_s$  is the average intensity of the signal, and  $\sigma_N$  is the variance of the Gaussian noise). Thus, the detection precision of the self-checking algorithm is very high.

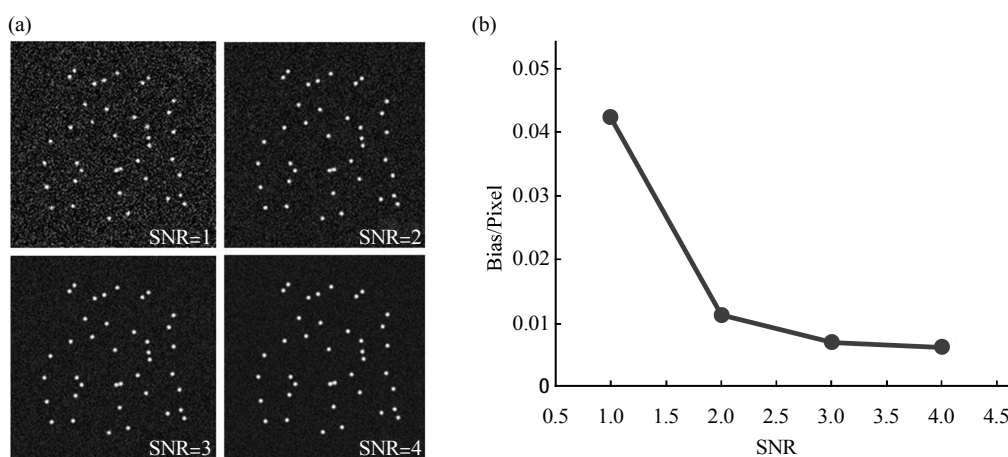


**Fig. 4 Bias of self-checking algorithm under different signal-to-noise ratio**

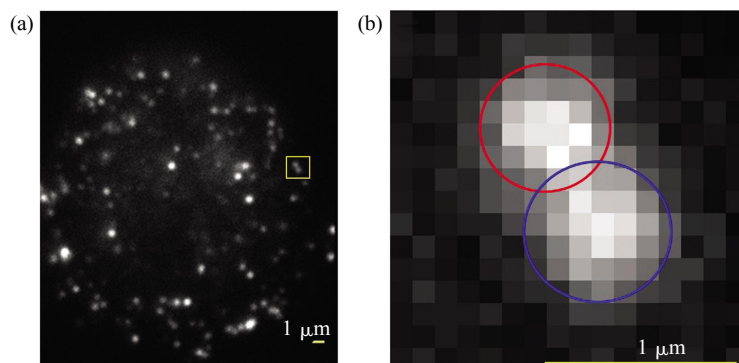
(a) Simulated images with signal-to-noise ratio 1, 2, 3, 4, respectively. (b) Bias versus signal-to-noise ratio curve.

We also carried out a test using mice  $\beta$  cell fluorescence images; Figure 5 is a fluorescence image of a  $\beta$  cell, acquired using total internal reflection fluorescence microscopy. Figure 5a is the fluorescence image of the  $\beta$  cell; the length of the scale bar in the figure is 1  $\mu\text{m}$ . An enlarged image of the vesicles in the yellow box is shown in Figure 5b. The image shown in Figure 5b is our testing area, and the red round box and blue round box areas in Figure 5b are vesicles recognized manually. First, we used the wavelet transform algorithm to preprocess the image to remove the background and noise, and then we applied the watershed algorithm and the watershed algorithm plus the self-checking algorithm to test detection effects. Figure 6 is a comparison of the quantities of vesicles detected in the Figure 5b area using the watershed algorithm and the watershed algorithm plus

the self-checking algorithm. From Figure 6, it can be seen that the detected vesicle quantity using the watershed algorithm in the same area fluctuated between 1 and 2, whereas the detected vesicle quantity of the watershed algorithm plus the self-checking algorithm remained steadily at 2. We traced the vesicles continuously for 100 frames in the Figure 5b area and drew the  $x$  coordinate of the traced vesicle central position versus the time curve. Figure 7a is the  $x$  coordinate of the traced vesicle central position versus the time curve for the watershed algorithm plus the self-checking algorithm. Figure 7b is the  $x$  coordinate of the traced vesicle central position versus the time curve for the watershed algorithm. From Figure 7a, it can be seen that the self-checking algorithm can trace the completed trajectory of two vesicles due to its high accuracy. However, without the

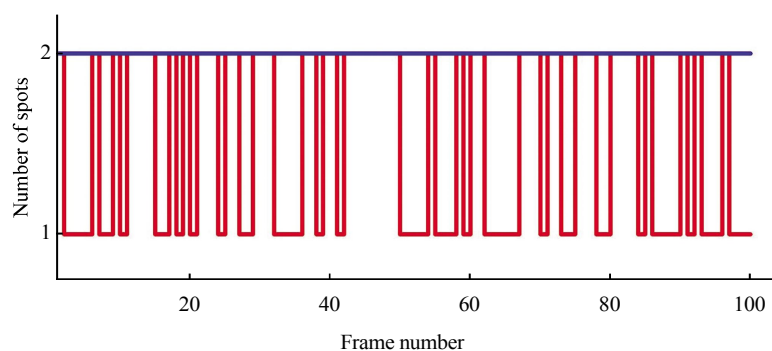
self-checking algorithm, the traced vesicle's trajectory is confusing because of detection error, as shown in

Figure 7b.



**Fig. 5 Fluorescence image of a  $\beta$  cell, acquired using total internal reflection fluorescence microscopy**

(a) The fluorescence image of the  $\beta$  cell. An enlarged image of the vesicles in the yellow box is shown in (b). The red round box and blue round box areas in (b) are vesicles recognized manually.



**Fig. 6 The number of vesicles detected in Figure 5b using the watershed algorithm and the watershed algorithm plus the self-checking algorithm**

— : Watershed; — : Watershed+SC.

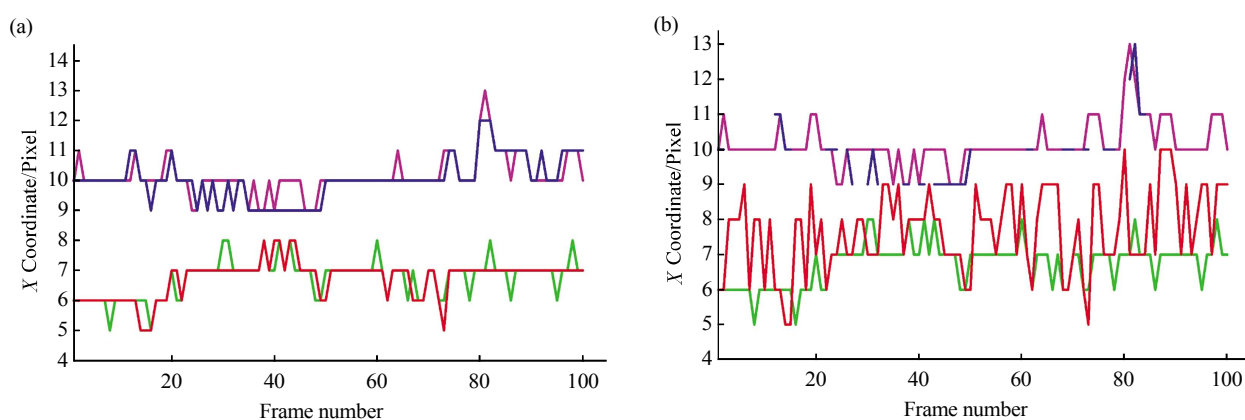


**Fig. 7 X coordinate of the traced vesicle central position versus the time curve**

(a) The  $x$  coordinate of the traced vesicle central position versus the time curve for the watershed algorithm plus the self-checking algorithm. Spot1-M and Spot2-M indicate the trace of Spot1 and Spot1 tracked manually. Spot1-C and Spot2-C indicate the trace of Spot1 and Spot1 tracked by computer. (b) The  $x$  coordinate of the traced vesicle central position versus the time curve for the watershed algorithm. — : Spot1-M; — : Spot2-M; — : Spot1-C; — : Spot2-C.

Based on the result of the above analysis, we can confirm that after joining the self-checking algorithm, the accuracy of the vesicle detection in biological fluorescence images was improved. Therefore, we proposed an optimized flow chart of vesicle tracking analysis as showing in Figure 8.

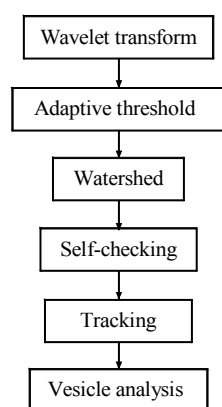


Fig. 8 Flow chart of vesicle tracking analysis

First, wavelet transform algorithm was used to remove the noise and background in fluorescence images. Then vesicles were segmented from binary images by adaptive threshold algorithm. However, only fixed threshold was difficult to separate close vesicles, and it need to use watershed algorithm to separate close vesicles. The centroids of well-segmented vesicles were calculated in this step, and self-checking algorithm was used to optimize detection of vesicles further. Finally, we can use optimized data to tracked vesicles and analyze the traces. Many multiple particle tracking algorithm was proposed in previous studies<sup>[24-25]</sup>. In this paper, we use the scheme of Kalman filter and linear assignment problem to track the vesicles<sup>[12]</sup>. According to the procedure of vesicle tracking, we analyzed data of mice  $\beta$  cells before and after glucose stimulation as shown in Figure 9.

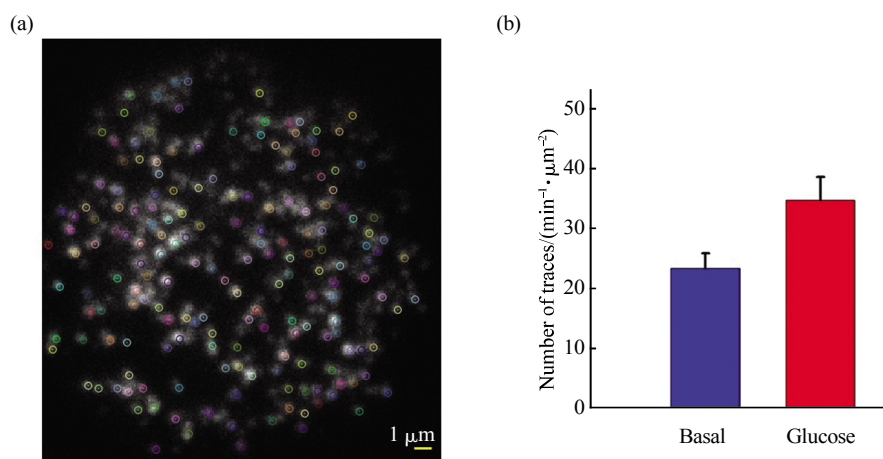


Fig. 9 Vesicle tracking analysis of mice  $\beta$  cells

(a) View of the vesicle tracks superimposed on fluorescence image. The color circles indicated the detection of the vesicle tracks. (b) Comparison of the number of vesicle traces before and after glucose stimulation. Data represent the number of traces detected per  $100 \text{ min}^{-1} \cdot \mu\text{m}^{-2}$  from 4 cells in each state. ■: Basal; ■: Glucose.

From Figure 9b, we can see that the number of vesicle traces was significantly increased after glucose stimulation, which indicated that there were more vesicles trafficking to the membrane after glucose stimulation in mice  $\beta$  cells. The function of these vesicles was to promote the release of insulin to regulate glucose balance. This result was coincident with previous studies<sup>[26]</sup>. In condition of high glucose, the pancreas of body will release insulin to regulate

blood sugar balance. Meanwhile, we made a statistical analysis of docking time before and after glucose stimulation, as shown in Figure 10.

From the docking time histogram of before and after glucose stimulation, we can see that the events with docking time less than 5 seconds increased significantly after glucose stimulation, which indicated that glucose stimulation accelerated vesicle translocation and secretion in  $\beta$  cell. Average docking

time and cumulative frequency before and after glucose stimulation were compared in Figure 10c and Figure 10d. In combination with Figure 9b, we came to a conclusion that the number of vesicle traces increased and the average docking time of vesicles decreased after glucose stimulation. This is because  $\beta$

cells will release insulin to regulate glucose balance with the help of vesicle translocation and secretion after glucose stimulation. In a word, we quantified the vesicles activity in mice  $\beta$  cell by tracking analysis on subcellular level.

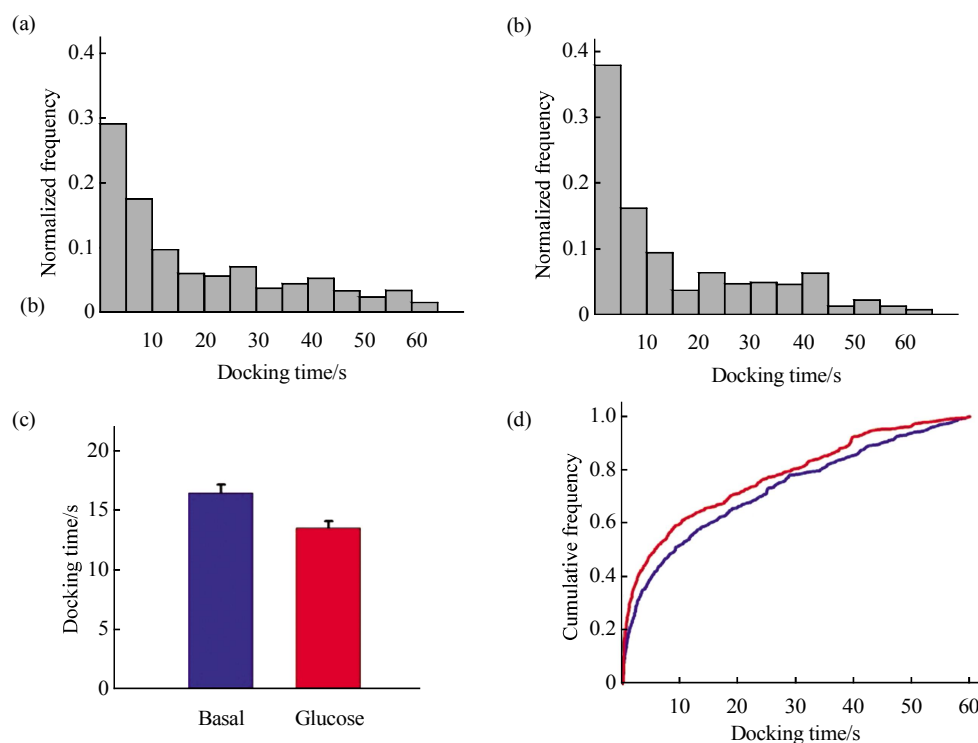


**Fig. 10** Statistical analysis on docking time before and after glucose stimulation

(a) Normalized docking time histogram from 4 cells in basal state. (b) Normalized docking time histogram from 4 cells after glucose stimulation. (c) Comparison of docking time before and after glucose stimulation (Kolmogorov-Smirnov test,  $P < 10^{-3}$ ). ■: Basal; ■: Glucose. (d) Cumulative frequency of docking time in two state. —: Basal; —: Glucose.

### 3 Discussion

In biological study, it is often necessary to observe the dynamic movements of vesicles in cells; when we mark vesicles with fluorescent protein, the dynamic movement of vesicles can be recorded by using a total internal reflection fluorescence microscope. Then, we can obtain much valuable information through the analysis of the dynamic movements of vesicles. Because manually analyzing a large number of vesicles is time-consuming and exhausting, automatic algorithms are necessary to speed up the process. At present, many algorithms are used to detect vesicles in fluorescence images. However, we find that it is difficult to detect all vesicle

movement trajectories correctly using time series images. The main reason for error tracking is the incorrect detection of vesicles. We detected the central positions of the vesicles and then connected these vesicles to form a movement trajectory by using the tracking algorithm. The reason for the incorrect detection of vesicles is that vesicles may be very close at some times during their dynamic movement, which is a challenge for many algorithms. Therefore, in this paper, we proposed a self-checking algorithm to correct the detection error of other algorithms to improve detection accuracy.

In the paper, we make a comparison of the detection accuracy of the wavelet transform algorithm, local maximum algorithm and watershed algorithm, as

well as these algorithms plus the self-checking algorithm. We find that when the center distance of the two vesicles is more than 6 pixels, all algorithms can detect them correctly. When the distance between two vesicles is less than 6 pixels, the detection accuracy of the wavelet transform algorithm drops to approximately 0%. The wavelet transform algorithm is one of the segmentation algorithms based on a threshold, which means that when the distance between two spots is very small, the segmentation algorithm based on a threshold has difficulty separating them correctly. However, the local maximum algorithm and watershed algorithm can distinguish vesicles that are very close to some extent. When the distance between two vesicles is less than 3 pixels, the detection accuracy drops below 50%. When the center distance of two vesicles is less than 2 pixels, the detection accuracy is less than 10%. The detection accuracy of these algorithms improves greatly after adding the self-checking algorithm. Moreover, after adding the self-checking algorithm, the detection accuracies of the local maximum algorithm and watershed algorithm are improved from less than 10% to above 80% for the pixel interval of [2,3) and from less than 50% to above 90% for the pixel interval [3,4). Thus, the improvement is very obvious.

In this paper, we also tested the detection accuracy of the self-checking algorithm under different vesicle densities and different maximum movement speeds, and from the results, we can see that different parameters have little impact on the self-checking algorithm's detection accuracy. We also tested the average detection precision of the self-checking algorithm with different signal-to-noise ratio, and we found that the average detection precision of the self-checking algorithm is less than 0.05 pixels.

Meanwhile, we analyzed two adjacent vesicles in mice  $\beta$  cell fluorescence images. First, we used the wavelet transform algorithm to preprocess the image to remove the background and noise, and then we applied the watershed algorithm to detect vesicles. Moreover, it was found that the number of vesicles detected by the watershed algorithm fluctuated between 1 and 2 during the 100 frames. After adding the self-checking algorithm, all frames could detect the two vesicles correctly. Moreover, the watershed algorithm plus the self-checking algorithm could track the completed movement trajectories of the two vesicles by using the tracking algorithm. Without the self-checking

algorithm, the traced vesicle trajectories were confusing because of detection error.

Finally, we proposed an optimized flow chart of vesicle tracking and analyzed vesicle traces in mice  $\beta$  cell before and after glucose stimulation. We came to a conclusion that the number of vesicle traces increased and the average docking time of vesicles decreased after glucose stimulation based on our tracking analysis. This is because  $\beta$  cells will release insulin to regulate glucose balance with the help of vesicle translocation and secretion after glucose stimulation. In a word, we quantified the vesicles activity in mice  $\beta$  cell by tracking analysis on subcellular level.

To sum up, the detection accuracy is greatly improved *via* the self-checking algorithm. Moreover, the detection precision of the self-checking algorithm is very high. When we apply the self-checking algorithm to mice  $\beta$  cell fluorescence images, it can also detect the completed movement trajectory of vesicles correctly. Therefore, the self-checking algorithm can be used to detect and track objects in biological fluorescence images to improve the accuracy of analysis.

**Ethics Statement** Animal experimentation: This study was performed in strict accordance with the recommendations in the Guide for the Care and Use of Laboratory Animals of Institute of Biophysics, Chinese Academy of Sciences. All of the animals were handled according to approved institutional animal care and use committee (IACUC) protocols of the Institute of Biophysics. All experiments were approved by the Animal Care Committee at the Institute of Biophysics (license number: SYXK2016-19). All surgery was performed under sodium pentobarbital anesthesia, and every effort was made to minimize suffering.

## References

- [1] Bai L, Wang Y, Fan J, *et al.* Dissecting multiple steps of GLUT4 trafficking and identifying the sites of insulin action. *Cell Metabolism*, 2007, **5**(1): 47–57
- [2] Oheim M, Stuhmer W. Tracking chromaffin granules on their way through the actin cortex. *European Biophysics Journal*, 2000, **29**(2): 67–89
- [3] Oharaimaizumi M, Nakamichi Y, Tanaka T, *et al.* Imaging exocytosis of single insulin secretory granules with evanescent wave microscopy: distinct behavior of granule motion in biphasic insulin release. *Journal of Biological Chemistry*, 2002, **277** (6): 3805–3808

- [4] Huet S, Karatekin E, Tran V, *et al.* Analysis of transient behavior in complex trajectories: application to secretory vesicle dynamics. *Biophysical Journal*, 2006, **91**(9): 3542–3559
- [5] Li C, Bai L, Li D, *et al.* Dynamic tracking and mobility analysis of single GLUT4 storage vesicle in live 3T3-L1 cells. *Cell Research*, 2004, **14**(6): 480–486
- [6] Sezgin M, Sankur B. Survey over image thresholding techniques and quantitative performance evaluation. *Journal of Electronic Imaging*, 2004, **13**(1): 146–168
- [7] Otsu N. A threshold selection method from gray level histograms. *IEEE Transactions on Systems*, 1979, **9**(1): 62–66
- [8] Olivomarin J. Extraction of spots in biological images using multiscale products. *Pattern Recognition*, 2002, **35**(9): 1989–1996
- [9] Bright D, Steel E. Two - dimensional top hat filter for extracting spots and spheres from digital images. *Journal of Microscopy*, 1987, **146**(2): 191–200
- [10] Starck J, Murtagh F, Bijouai A. *Multiresolution Support Applied to Image Filtering and Restoration*. USA: Academic Press Inc, 1995
- [11] Sadler B, Swami A. Analysis of multiscale products for step detection and estimation. *IEEE Transactions on Information Theory*, 1999, **45**(3): 1043–1051
- [12] Jaqaman K, Loerke D, Mettlen M, *et al.* Robust single particle tracking in live cell time-lapse sequences. *Nature Methods*, 2008, **5**(8): 695–702
- [13] Pecot T, Bouthemy P, Boulanger J, *et al.* Background fluorescence estimation and vesicle segmentation in live cell imaging with conditional random fields. *IEEE Transactions on Image Processing*, 2015, **24**(2): 667–680
- [14] Liu B, Xue Y, Zhao W, *et al.* Three-dimensional super-resolution protein localization correlated with vitrified cellular context. *Scientific Reports*, 2015, **5**: 13017–13027
- [15] Smith C S, Stallinga S, Lidke K A, *et al.* Probability-based particle detection that enables threshold-free and robust *in vivo* single-molecule tracking. *Molecular Biology of the Cell*, 2015, **26**(22): 4057–4062
- [16] Jaiswal A, Godinez W J, Eils R, *et al.* Tracking virus particles in fluorescence microscopy images using multi-scale detection and multi-frame association. *IEEE Transactions on Image Processing*, 2015, **24**(11): 4122–4136
- [17] Crocker J, Grier D. Methods of digital video microscopy for colloidal studies. *Journal of Colloid and Interface Science*, 1996, **179**(1): 298–310
- [18] Feng L, Xu Y, Yang Y, *et al.* Multiple dense particle tracking in fluorescence microscopy images based on multidimensional assignment. *Journal of Structural Biology*, 2011, **173**(2): 219–228
- [19] Bricard A, Caussin J, Desreumaux N, *et al.* Emergence of macroscopic directed motion in populations of motile colloids. *Nature*, 2013, **503**(7474): 95–98
- [20] Meyer F. Topographic distance and watershed lines. *Signal Processing*, 1994, **38**(1): 113–125
- [21] Peng A, Rotman Z, Deng P, *et al.* Differential motion dynamics of synaptic vesicles undergoing spontaneous and activity-evoked endocytosis. *Neuron*, 2012, **73**(6): 1108–1115
- [22] Lizunov V A, Matsumoto H, Zimmerberg J, *et al.* Insulin stimulates the halting, tethering, and fusion of mobile GLUT4 vesicles in rat adipose cells. *The Journal of Cell Biology*, 2005, **169**(3): 481–489
- [23] Baltrusch S, Lenzen S. Monitoring of glucose-regulated single insulin secretory granule movement by selective photoactivation. *Diabetologia*, 2008, **51**(6): 989–996
- [24] Reid D B. An algorithm for tracking multiple targets. *IEEE Transactions on Automatic Control*, 1979, **24**(6): 843–854
- [25] Jonker R, Volgenant A. A shortest augmenting path algorithm for dense and sparse linear assignment problems. *Computing*, 1987, **38**(4): 325–340
- [26] Rhodes C J, Halban P A. Newly synthesized proinsulin/insulin and stored insulin are released from pancreatic B cells predominantly *via* a regulated, rather than a constitutive, pathway. *Journal of Cell Biology*, 1987, **105**(1): 145–153

# 时间序列荧光图像中精确检测高密度快速运动多囊泡的“自校正”算法\*

张翔<sup>1,2)\*\*</sup> 刘欣怡<sup>2)</sup> 吕平平<sup>2)</sup> 贾策<sup>2)</sup>

(<sup>1)</sup> 华中科技大学生命科学与技术学院, 武汉 430074; (<sup>2)</sup> 中国科学院生物物理研究所, 北京 100101)

**摘要** 本文提出了一种“自校正”算法, 用于提高时间序列荧光图像中的多个运动目标识别的正确率(如囊泡). 此算法的主要思想是构建一个由核函数叠加构成的模型, 然后用这个模型去拟合无法分辨时刻的数据, 通过最小二乘拟合后得到的模型与真实数据的 $\chi^2$ 统计残差及拟合得到的核函数的参数, 来确定该时刻囊泡的数目及各囊泡的中心位置. 我们在合成图像上比较加入了自校正算法和未加自校正算法的识别正确率, 结果表明, 加入了自校正算法以后识别正确率得到了明显提高. 同时, 提出了一个优化的囊泡追踪流程, 并应用到小鼠 $\beta$ 细胞的囊泡荧光图像分析中. 统计分析显示, 加入葡萄糖刺激后, 小鼠 $\beta$ 细胞囊泡轨迹数目会增加, 平均锚定时间会减少, 这是由于胰岛细胞需要借助囊泡的转运和分泌来调控血糖平衡. 因此我们进一步在亚细胞水平定量分析了活细胞中囊泡的活动.

**关键词** 自校正算法, 囊泡追踪, 囊泡识别, 时间序列图像

**学科分类号** Q334, Q336

**DOI:** 10.16476/j.pibb.2017.0046

\* 国家自然科学基金资助项目(31300701).

\*\* 通讯联系人.

Tel: 010-64888523, E-mail: zhangxiang@moon.ibp.ac.cn

收稿日期: 2017-02-13, 接受日期: 2017-03-30